J. Earth Syst. Sci. (2020)129 45
https://doi.org/10.1007/s12040-019-1302-7

Compositional mapping and the evolutionary history of Mare Tranquillitatis

H Bhatt[1,3,*], P Chauhan[2] and P Solanki[1]

[1]*Geology Department, M.G. Science Institute, Ahmedabad, Gujarat, India.*
[2]*Indian Institute of Remote Sensing, ISRO, Dehradun, Uttarakhand, India.*
[3]*Research Scholar, Gujarat University, Ahmedabad 380 009, India.*
**Corresponding author. e-mail: henalbhatt@yahoo.in*

MS received 3 March 2019; revised 16 August 2019; accepted 23 September 2019

This study signifies the compositional variability of Mare Tranquillitatis basalt and the Irregular Mare patches (IMPs) – the youngest volcanic feature on the Moon, using hyperspectral data from Moon Mineralogy Mapper (M^3) for the first time. Along with composition, the topographic and morphological mapping has been done to understand the possible evolutionary history of this mare. Total 22 spectral units has been identified based on Integrated Band Depth (IBD) parameter technique. Number of reflectance spectra were collected from the fresh craters of each spectral unit and quantitative mineralogical abundances estimated using band parameters like band centre, band strength and band area. The result shows abundances of olivine and pyroxene mixture bearing material in the mare basalt. The compositional map shows smaller spectral units in the western-low lying half and larger spatial distribution of spectral unit in the eastern half depicts probable large-scale volcanic eruption in the eastern part that may have flowed to longer distances from the Cauchy shield to the central mare. This study marks 61 new domes in the Cauchy shield area and also depicts possible formation and evolutionary history of the Mare Tranquillitatis.

Keywords. Lunar surface; compositional mapping; Mare Tranquillitatis; hyperspectral remote sensing; the shield volcano.

1. Introduction

The study of compositional variation of a terrestrial surface based on remote sensing and reflectance spectroscopy has been done from five decades. The mineralogical diversity of the mare surface reveals the heterogeneous nature of the lunar upper mantle, which is the source region of the mare basalts (Pieters 1993). Basaltic magmas are produced by partial or impact-induced partial or complete melting of near-surface rock (Basaltic Volcanism Study Project (BVSP) 1981). Even though Lunar basalts are comprising <1% of the Lunar crust (Head 1976), these are surficial treasure of the Moon as it reveals geological history, thermal history and subsequent evolution of Moon. Basalts are formed from partial melt of planetary interiors and provide a detailed information on the geochemistry and mineralogy of their source regions (BVSP 1981). The bulk of basaltic magmatism on the Moon

Supplementary materials pertaining to this article are available on the Journal of Earth Science Website (http://www.ias.ac.in/Journals/Journal_of_Earth_System_Science).

Published online: 04 January 2020

occurred from 3.9 to 3.1 Ga ago on the ancient plains (BVSP 1981). However, recent investigations showed the presence of younger volcanic activity within last ∼0.1 Ga (Braden *et al.* 2014; Elder *et al.* 2017). Spectral diversity from the remote sensing analysis of unsampled mare basalt suggests that Lunar basalt and their source region are more heterogeneous compared to sample returned (Pieters 1993). Lunar volcanism appears to be multiphase and complex irrespective of the neighbouring region (Pieters 1993; Chauhan *et al.* 2012). Analysis of returned samples from Apollo and Luna mission suggests that Lunar basalts are composed of pyroxenes, feldspar, olivine and Fe–Ti oxide bearing ilmenite, spinel, armalcolite (BVSP 1981).

Olivine and Pyroxene are two most abundant mafic minerals present in the lunar surface. Pyroxene is the most abundant mineral of the basalt which is characterized by their unique dual absorption features at 1 and 2 μm, due to electronic transition of Fe^{+2} and Ca^{+2} situated in the M1 and M2 crystallographic site of mineral crystal (Burns 1993). Olivine exhibit three overlapping absorption feature centered between 1.05 and 1.10 μm and lacks 2 μm absorption feature (Adams 1975; Singer 1981; King and Ridley 1987; Burns 1993). These three overlapping features at band I rises due to crystal field transition in Fe^{+2} located at M1 and M2 crystallographic sites, where the central band is attributed to Fe^{+2} in the M2 site and two-side bands are attributed to Fe^{+2} in the M1 site. The band center in olivine increase to longer wavelength with increasing Fe^{+2} content (King and Ridley 1987; Burns 1993). The spectral absorption of pyroxene is dominating even if present in minor amount. As an example, minor abundances of pyroxene in the olivine–pyroxene mixture can be diagnosed by 2 μm absorption band and its presence obscures the 1 μm features of olivine, which remains indistinctive (Singer 1981; Burns 1989). It also masks the 1.25 μm absorption feature of plagioclase (Crown and Pieters 1987). Plagioclase is the second most abundant mineral in basalts, followed by olivine and ilmenite which varies from minor to 20% (Pieters and Englert 1997). Compositional mapping of Mare Tranquillitatis has been done by various researchers from 1995 on the basis of FeO and TiO_2 content (Papike *et al.* 1976; Johnson *et al.* 1991; Jerde *et al.* 1994; Melendrez *et al.* 1994; Bell and Hawke 1995; Lucey *et al.* 1995; Staid *et al.* 1996; Giguere *et al.* 2000; Gillis *et al.* 2003; Kodama and Yamaguchi 2003; Dhingra *et al.* 2010; Sato *et al.* 2017). In this study, we have analysed compositional heterogeneity based on major primary minerals of basalt-like pyroxene, plagioclase and olivine for Mare Tranquillitatis. Composition of Irregular Mare Patches is also studied in this work for the first time using hyper spectral data and along with composition, morphology of the mare is studied to understand possible evolutionary history of the mare.

2. Background

2.1 *Geology of Mare Tranquillitatis and previous work*

Mare Tranquillitatis is a nonmascon (Muller and Sjogren 1968; Zuber *et al.* 2013), pre-Nectarian aged basin (Wilhelms *et al.* 1987), located at 7°N, 30°E (figure 1), surrounded by Mare Crisium, Mare Fecunditatis, Mare Nectaris, Mare Vaporum and Mare Serenitatis and is well known for Apollo 11 landing site. According to the analysis of Apollo 11 returned samples, this region is mainly composed of basaltic mineralogy, deposited during the Imbrium to late Imbrium period (Wilhelms *et al.* 1987). It shows characteristic two-basin ring structure (Spudis 2005; De Hon 2017) with a diameter of ∼800 km from east to west (Staid *et al.* 1996) (figure 1). The eastern and western basins show subtle differences in topography and superposed features (De Hon 2017). Early telescopic data characterized Mare Tranquillitatis as darkest and bluest basalts (Pieters 1978). This characteristic bluish appearance compared to all other mare is ascribed to high TiO_2 content in the area and empirically related to UV/VIS reflectance ratio (Charette *et al.* 1974; Pieters 1978). Mare Tranquillitatis shows irregular boundary and is well known for its high titanium bearing basalts from both, ground-based Apollo 11 samples and remote sensing based analytical results (Papike *et al.* 1976; Johnson *et al.* 1991; Jerde *et al.* 1994; Melendrez *et al.* 1994; Bell and Hawke 1995; Lucey *et al.* 1995; Staid *et al.* 1996; Giguere *et al.* 2000; Gillis *et al.* 2003; Kodama and Yamaguchi 2003; Dhingra *et al.* 2010; Sato *et al.* 2017). Samples returned from Apollo 11 and Apollo 17 are the highest Titanium bearing and pristine basalts (Papike *et al.* 1976; Beaty and Albee 1978; Nyquist and Shih 1992). High concentration of Titanium in the basalt requires high ilmenite bearing source region and indicates its late-stage magmatic fractionation from Lunar Magma Ocean (LMO) (Snyder *et al.* 1992). Pieters (1978) classified mare basalts into three types based on UV/VIS ratio,

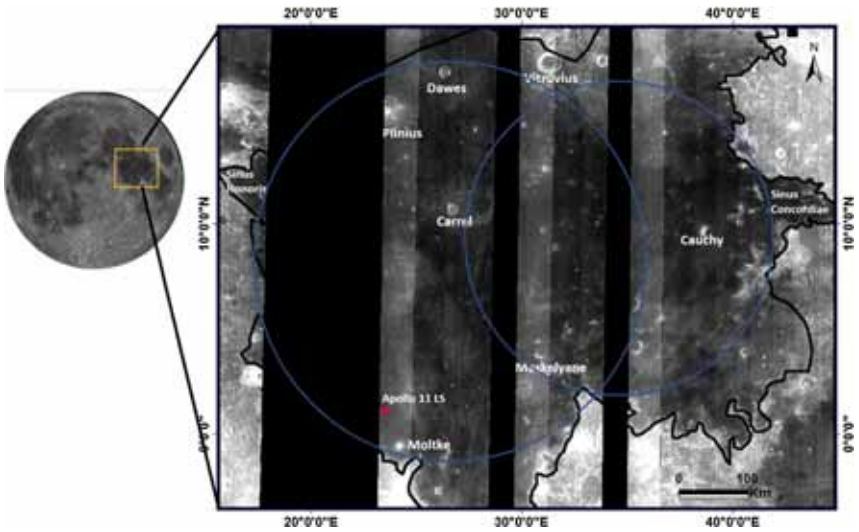

Figure 1. M^3 mosaic of Mare Tranquillitatis generated using data from OP1A and OP1B, 100 km orbital altitude, presenting the 750 nm albedo image. Black vertical part shows the gap in data coverage by M^3 payload. Major craters and Apollo 11 landing site in Mare Tranquillitatis are labelled. Blue circles marks two basin model as per De Hon (2017).

albedo, 1 μm band strength and 2 μm absorption band presence. Most of the mare is classified into HDWA (High UV/VIS ratio, Dark albedo, Weak 1 μm band, Absence of 2 μm band), and hDWA (Medium to high UV/VIS ratio, Dark albedo, Weak 1 μm band, Absence of 2 μm band) basalts, and the third is mIG type (medium UV/VIS ratio, Intermediate albedo, General 1 μm band), which is deposited on the south-western and the north-eastern part of the mare. Heisinger *et al.* (2000) estimated the surface ages of Mare Tranquillitatis using Apollo and Lunar orbiter high resolution data and Crater Size Frequency Distribution (CSFD) method, which is dominated by single peak volcanism in the number of erupted units during 3.6–3.8 Ga. This study represents the geological investigation of 38 sites of IMPs (Irregular Mare Patches) within the Mare Tranquillitatis, which have been recognised recently to be the evidence of latest volcanic activity on the lunar surface (Braden *et al.* 2014; Elder *et al.* 2017) (figure 8). These IMPs are small irregular morphologies recognised as uneven and smooth deposits, ranges in dimension from 100 to 5000 m and paucity of superimposed impact craters with >10 m diameter (Braden *et al.* 2014). These features are hypothesized to be originated due to pyroclastic explosive eruption or removal of material by outgassing (Elder *et al.* 2017).

2.2 *Geomorphology of the area*

The area shows various structural and morphological features such as the presence of long rille, wrinkle ridges, domes, collapsed pit and faults (figure 9). Mare Tranquillitatis represents the largest shield volcano on the Moon (Spudis *et al.* 2013). Using LRO LOLA data, Spudis *et al.* (2013) investigated the eastern topographic upliftment of the area as the largest shield volcano, Cauchy shield with 1.8 km relief. This shield displays volcanic landforms such as low shield with a summit pit. Rima Cauchy rille is a 210 km long graben at north of Cauchy crater. Rupes Cauchy is ∼120 km long fault which forms a series of cliffs or escarpments below the Cauchy crater. At the northern end of the Cauchy structure, there is a smaller feature identified as the Gardner 'megadome' by Wood (2003). This small (∼70 km; 16°N, 34°E) topographic blister displays several smaller, overlapping shields and sinuous rilles. Its summit displays a series of irregular depressions that may construct a caldera complex. The Gardner shield is relatively small, but shows the topographic relief of about 1.6 km. Both the shields do not show genetic relation (Spudis *et al.* 2013). Tye and Head (2013) have mapped 115 mare domes using LOLA data in the eastern part of this shield. Within the basin, these domes form linear cluster parallel to the north-western end of Rima Cauchy, indicates a possible genetic relationship. Tye and Head (2013) suggest that the eastern rise was formed by infrequent, high-volume episodes which flooded areas beyond the rise itself. These qualities distinguish its eruption style from that of a terrestrial shield volcano and may make it better understood as a lava plateau (Tye and Head 2013). Recent gravity data from the GRAIL (Gravity Recovery and

Interior Laboratory) mission, indicate that there is no basin-wide positive Bouguer gravity anomaly, which sets this basin apart from most other known basins and indicates that mantle uplift is not likely to be a contributor to the elevation of the broad rise (Zuber *et al.* 2013). Li *et al.* (2018) have mapped wrinkle ridges of Mare Tranquillitatis and its average formation time 2.4 Ga which is 1.4 Ga after its oldest surface lavas, a significantly longer period than for any other basin.

3. Data used

High-resolution hyperspectral data from Moon Mineralogy Mapper (M^3) (Goswami and Annadurai 2009; Boardman *et al.* 2011) instrument onboard India's first Lunar mission – Chandrayaan-1 is used for the compositional analysis. M^3 operate in VNIR spectral region, ranging from 540 to 3000 nm with 85 contiguous bands and has 140 m/pix spatial resolution at 100 km orbital altitude (Pieters *et al.* 2009). M^3 level-2 data which is pixel located, thermally corrected, photometrically corrected (Clark *et al.* 2011; Besse *et al.* 2013), reflectance data with optical period-OP1A and OP1B from the 100 km orbital altitude is acquired from PDS Geoscience node (https://ode.rsl.wustl.edu/moon/indexProductSearch.aspx). List of the dataset used is given in appendix I in the supplementary file. Total of 22 image scenes were georeferenced and mosaicked, which is shown in figure 1. To study the topography of the area, Lunar Orbiter Laser Altimeter (LOLA) Digital Elevation Model (DEM) data of 1024 pixel/degree resolution from Lunar Reconnaissance Orbiter (LRO) mission was acquired from PDS Geoscience Node (https://ode.rsl.wustl.edu/moon/indexProductSearch.aspx). To study major morphologic features of the mare, Lunar Reconnaissance Orbiter Camera (LROC) Wide Angle Camera (WAC) 100 m data of the Lunar Reconnaissance Orbiter (LRO) is used and is acquired from https://astrogeology.usgs.gov.

4. Methodology

4.1 *Integrated band depth (IBD) technique*

To study the mineralogical variations of Mare Tranquillitatis, Integrated Band Depth (IBD) parameter technique has been used. The IBD parameter is defined for characterizing the band depths for 1- and 2-μm absorption features in order to capture the spectral variations related to mafic minerals, soil maturity and space weathering (Mustard *et al.* 2011). The IBD for 1- and 2-μm absorption features is defined as the total integrated band depth calculated using equations given by Mustard *et al.* (2011). To calculate absorption band strength/depth from the reflectance spectra of the lunar materials requires removal of the continuum slope imparted by the space weathering process. Continuum removal has been performed by using the convex hull method given by Clark and Roush (1984). The IBD mosaic of Mare Tranquillitatis has been generated from M^3 mosaic by removal of the continuum and subsequent calculation of IBD parameter for 1- and 2-μm absorption feature. The 1.578 μm wavelength region is free from any Lunar mafic silicate absorption, therefore the IBD parameter mosaic of 1- and 2-μm band depths together with albedo band at 1.578 μm captures the surface mineralogical variations. IBD False Colour Composite (FCC) has been prepared by assigning a red channel to IBD-1, green to IBD-2 and blue to the 1.578 μm M^3 albedo channel (figure 2). This colour composite is used to characterize spectral diversity across the mare basins, which represents the net effect of composition, maturity and contamination by the highland materials. Using the integrated band depth parameter, the basaltic units of Mare Tranquillitatis have been delineated based on visually found colour variation in the false colour composite image generated using IBD parameters.

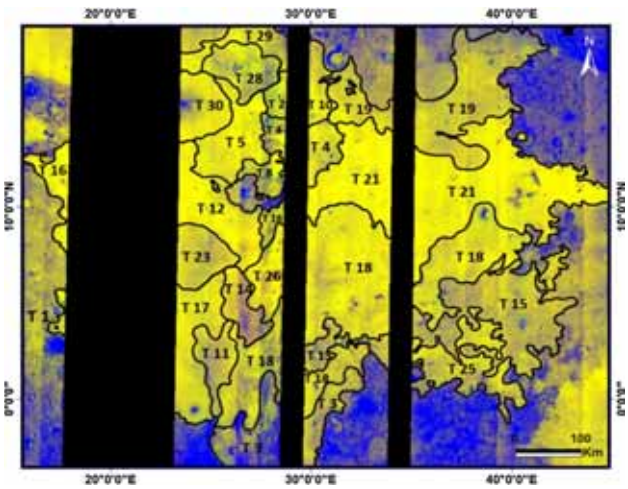

Figure 2. IBD mosaic of Mare Tranquillitatis generated using M^3 100 km altitude reflectance global datasets. Black lines demarcate the boundaries of the spectral units mapped in the study area (R: IBD 1 μm, G: IBD 2 μm, B: 1.578 μm).

4.2 *Collection of spectra*

To map the spectral variability of basalt units, the fresh crater of ∼1 km diameter is selected (Kaur *et al.* 2013; Chauhan *et al.* 2018). The diameter of the crater has been determined from the LROC quick-map site (https://quickmap.lroc.asu.edu). For each basaltic unit, number of fresh craters have been selected based on optical immaturity trend of each unit that is determined using 950/750 nm *vs.* 750 nm plot as documented in Lucey *et al.* (1995) and Wilcox *et al.* (2005). The average spectral reflectance profile of 2∗2 pixels from each selected fresh crater of each unit and utilized in spectral analysis. These spectral units are designated based on its chronological order from Hiesinger *et al.* (2000). Representative average reflectance spectral profile for each basaltic unit is shown in figure 3. Figure 3(a, c and e) are normalized reflectance spectra for units T-1 to T-30 and figure 3(b, d and f) are continuum removed reflectance spectra for units T-1 to T-30. All the other spectra of each unit are appended after unit name as: a, b, c (e.g., T-1 a, T-2 a, T-3 a, T-3 b; supplementary table S1). The details of spectral units, age, location information and details of band parameters computed for the spectral analysis are presented in appendix II. Spectral reflectance profiles from irregular mare patches is collected very carefully using M^3 data (figure 7) and the details of spectral IMPs and its spectral location is given in appendix III.

4.3 *Spectral parameter acquisition*

The basaltic units defined by their ages are analysed on the basis of quantitative abundance of their composition. To study the quantitative abundances of mafic mineral we calculated band parameters, i.e., band centre, band strength and band area. The relationship of band parameters and quantitative mafic mineral abundances is explained by Adams (1974), Cloutis and Gaffey (1991a), Gaffey *et al.* (2002), and Klima *et al.* (2007, 2011a, b). Band parameters have been calculated by fitting the 4th order polynomial fit to each spectra after the continuum removal process by fitting a straight-line continuum tangent on

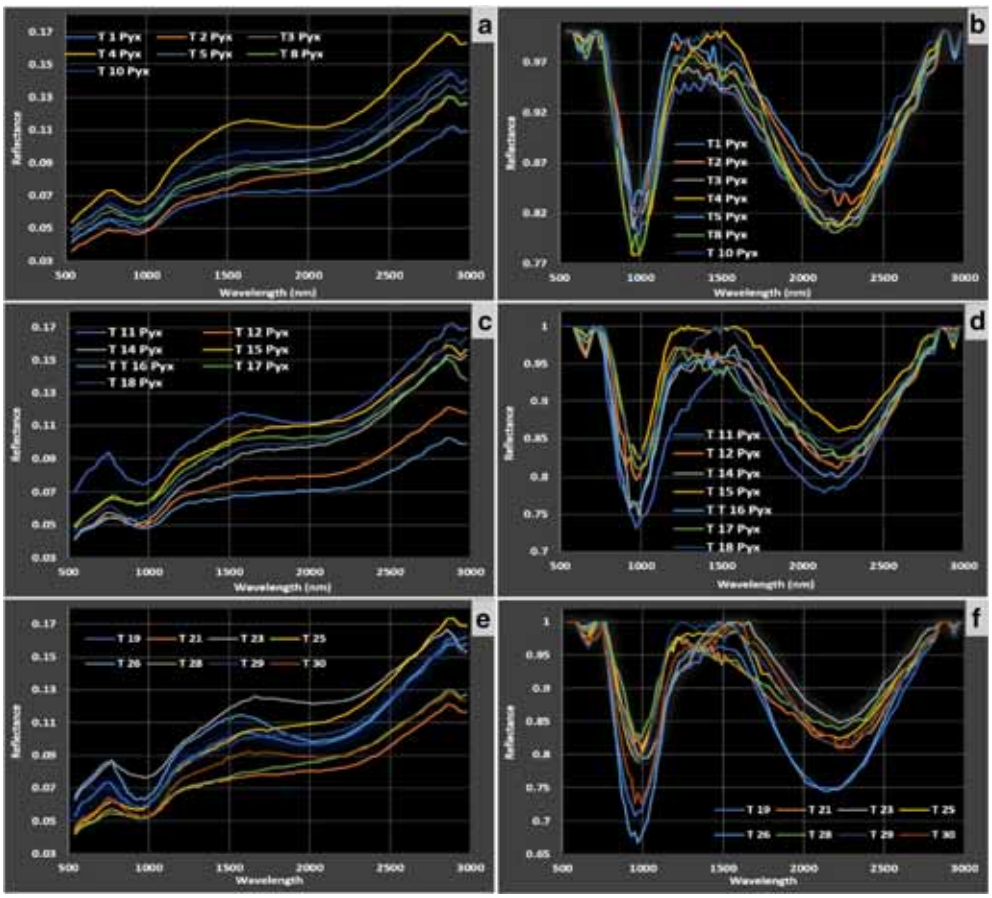

Figure 3. Representative average reflectance spectra from each of the unit. **a**, **c** and **e** are normalized reflectance spectra for unit 1 to 30 and **b**, **d** and **f** is continuum removed spectra of corresponding spectra in the graph **a**, **c** and **e**.

both sides of the absorption band for the Bands I and II separately and dividing the spectra by the respective continuum (appendix II). The highest reflectance point or shoulder maxima on both the sides of absorption feature is considered as tangent point. Band II is considered up to 2.5 μm. Band centre can be defined as lowest reflectance over a specific interval after continuum removal which is a key for mineral identification. As an example, quantitative information for pyroxene abundances can be inferred from Band I and Band II centre of reflectance spectra (Klima *et al.* 2007). Band depth is the length of a vertical line expressed in percent reflectance, which extends downward tangentially from 100% reflectance to the derived centre or minima (Clark and Roush 1984). Band area is a measure of the area of the absorption bound which has isolated the absorption or can be explained as the area between continuum slope and the data points which gives information of relative mafic mineral abundances like olivine and/or pyroxene mixture and pyroxene chemistry. The average error in the computation of band parameter is ± 0.02. The resulting band parameter values for each spectral unit is presented in appendix II.

4.4 *Geomorphological study*

Spectral units were overlaid on the topographic map to study the possible evolutionary history of the area. Major volcanic and tectonic features such as, Sinus rille, Wrinkle ridges, faults, domes, collapsed pit are also mapped and presented in figures 8 and 9.

5. Result and discussion

5.1 *Spectral units and its characteristics*

There are 22 spectral units that have been categorized based on the variation in IBD parameter. The spatial distribution of these units can be observed in figure 2. In the IBD FCC image, yellow shade represents mare basaltic units while deep blue colour represents highland area surrounding the mare. Yellow colour shows variation in colour shading; based on which, we demarcated basaltic units within mare. Basaltic unit boundaries are matching with the age unit boundaries of the mare, analysed based on CSFD analysis by Hiesinger *et al.* (2000), except for two units lying at the south-east part (T-15 and T-25; figure 2). Based on this correlation, basaltic units are designated according to its chronological order from Hiesinger *et al.* (2000). The age of spectral unit is given in supplementary table S1. In the previous studies, this area was mapped based on FeO and TiO_2 wt% content which differs with model ages (Staid *et al.* 1996; Hiesinger *et al.* 2000; Sato *et al.* 2017). In this work, we segmented basaltic unit on the basis of IBD variations which can be correlated with model ages estimated by Hiesinger *et al.* (2000).

IBD FCC image shows major spatial distribution difference in the eastern and western units within mare. T-18 is the largest spatially distributed spectral unit beginning from eastern to central eastern to southern mare. T-21 is the second largest spectral unit which covers most part of Cauchy shield volcano. T-18 and T-21 units cover the major part of Cauchy shield volcano. T-15, T-19 and T-25 units are moderate in size in the eastern part, which show major highland contamination with pale blue to yellow colour. Central-western part show many small spectral segments, considering from north to south are T-29 at the boundary of Mare Serenitatis and Mare Tranquillitatis, T-28 covers the Dawes crater and its ejecta deposits, T-30 covers the Plinius crater and its ejecta deposits, T-2, T-4, T-8 and T-10 are smaller basaltic units. T-5, T-12, T-23, T-26, T-14, T-17 and T-11 show comparatively moderate spatial distribution. Dawes crater within T-23 unit shows well distributed prominent ejecta deposits and gives yellow to green colour within the crater. Unit T-17 covers the Apollo 11 landing site. Plinius crater and Moltke crater within spectral unit T-30 and T-17 excavate highland material. Carrel crater between unit T-8 and T-18 excavates highland material which appears blue coloured in IBD image and near to Carrel crater prominent highland kipukas are present which shows blue colour. T-21 unit near to Sinus Concordiae also shows highland kipukas.

5.2 *Spectral analysis*

To study the quantitative composition of spectral units, number of craters were sampled from each spectral unit. All the spectra display prominent absorption feature at 1 and 2 μm band which shows variations in band strength, band area and band centre. Band strength, band area and band centre from the continuum removed reflectance spectra of

each unit are calculated by fitting 4th order polynomial fit to each spectra using Matlab software and the resultant values are presented in appendix II, in supplementary file. Clinopyroxene exhibit B I center (∼0.96 to ∼1.05 μm) and B II center (∼2.1 to ∼2.4 μm) and orthopyroxene display B I center (∼0.90 to ∼0.94 μm) and B II center (∼1.8 to ∼2.1 μm) (Cloutis and Gaffey 1991b). Band I centre value for this mare varies from 0.958 to 1.004 μm except for the T-11a (0.938 μm) and Band II centre varies from 2.12 to 2.28 μm which indicates presence of clinopyroxenes in Mare Tranquillitatis. B I center is averaging ∼0.976 μm and B II center is averaging ∼2.209 μm, which signify presence of sub-calcic augite (∼0.99 and ∼2.18 μm; Cloutis and Gaffey 1991b) bearing material in the mare. Band I centre for the largest flowed unit T-18 and T-21 of the Cauchy shield varies from 0.958 to 0.996 μm. Band center values of each spectral unit is plotted in the Band II *vs.* Band I graph as per Klima *et al.* (2007, 2011a) along with synthetic orthopyroxene and clinopyroxene band center values from Klima *et al.* (2007, 2011a). Band I absorption is affected by binary mineral mixture of olivine and pyroxene (Adams 1974; Cloutis *et al.* 1986) and hence, it needs to be corrected by displacement of Band I center for olivine, as per Cloutis *et al.* (1986); Gaffey *et al.* (2002); and Chauhan *et al.* (2018), while studying pyroxene mineralogy (figure 4). All the band center values fall nearby and above the synthetic high to middle calcium pyroxene trend line which indicate presence of high to medium/sub-calcic pyroxene in the mare basalt. Recent analyses of Mare Tranquillitatis using high resolution Hyperspectral Imager data also indicates the presence of high calcium bearing material in this mare (Bhatt *et al.* 2018, 2019).

Band I strength for eastern units – the largest T-18 varies from 15% to 27%, for second largest unit T-21 varies from 14% to 17%, for T-19, 20% to 28%, for T-15, 16% to 23% and for T-25, 18% to 20%. Band strength for spectral units near to Apollo 11 site – T-17 (18%), T-11 (20% to 24%), T-23 (20%) and T-1 (17%). T-26 unit at the central part of mare shows highest band I strength up to 33% which also belongs to comparatively younger age of 3.46 b. y.

To study the mineralogical abundances of the mare basalt, band area ratio (BAR) was calculated by taking the ratio of Band area II *vs.* Band area I. BAR values were plotted against band I centre to estimate the relative abundance of mafic minerals like olivine and pyroxene (figure 5). Gaffey *et al.* (1993) had analysed quantitative mineralogical abundances for S-type asteroid and presented how the BAR *vs.* band I centre values can be interpreted for the mineralogical study. The heavy solid curve in figure 5 represents a simple olivine–pyroxene mixing line (Cloutis *et al.* 1986), BA rectangular zone presents pyroxene dominated basaltic achondrite assemblages, OL rectangular region comprises monomineralic olivine assemblages and the OC boot region presents mafic silicate components of ordinary chondrites (Gaffey *et al.* 1993). BAR values of Mare Tranquillitatis basalt ranges from 0.57 to 1.52, averaging ∼0.93. All the values of mare are clustering at the right part of the OC

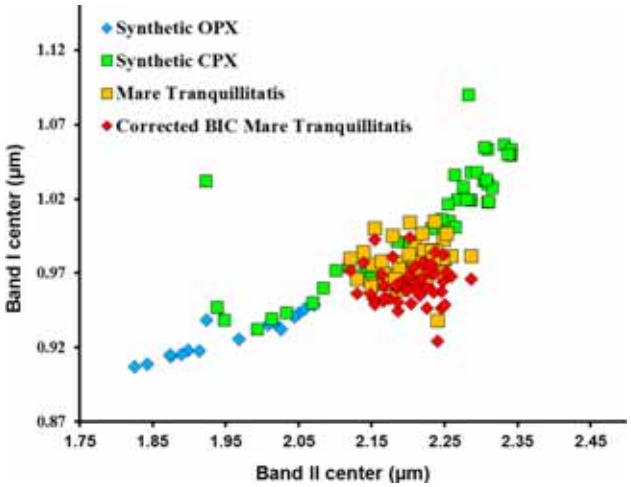

Figure 4. Plot of Band I centre data *vs.* Band II centre of the reflectance spectra of Mare Tranquillitatis. Synthetic pyroxene band centre from Klima *et al.* (2011a, b) has been plotted for comparative analysis of pyroxene of the mare.

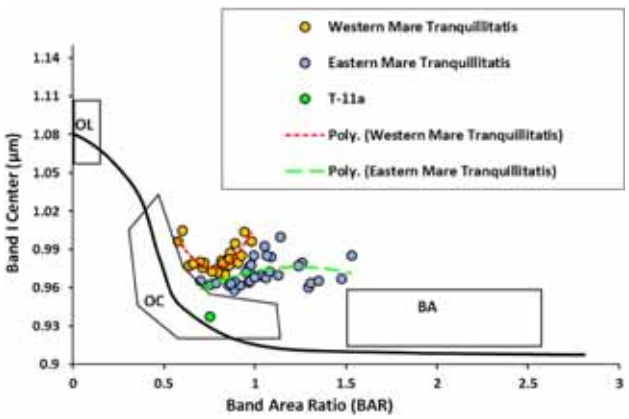

Figure 5. Band I centre *vs.* band area ratio (BAR) plot, modified after Gaffey *et al.* (1993), where OL is monomineralic olivine assemblage, OC represents mafic components of ordinary chondrites, BA rectangular zone represents pyroxene dominated basaltic achondrite assemblage. The solid curve represents olivine–pyroxene mixture line (Cloutis *et al.* 1986).

boot region in the BAR *vs.* B I plot, that indicates abundance of mafic silicate mixture in the area, particularly mixture of olivine and medium to high calcium bearing material. Presence of olivine in the olivine pyroxene mixture would affect band I center and B I area, as olivine spectra lacks Band II feature (Adams 1975; Singer 1981; Burns 1993). Band I center shift to longer wavelength if the small amount of olivine is present with pyroxene (Singer 1981). Olivine also shows additional absorption feature near 1.3 μm (Singer 1981). Olivine is less absorbing than pyroxene and hence, it is likely to be masked by pyroxenes unless it is present in good abundance (Singer 1981). Presence of pyroxene in the olivine pyroxene mixture can be identified by the band II absorption feature (Singer 1981). Clinopyroxene and olivine mixture spectra are less studied mafic silicate mixtures, due to lack of the laboratory data for this mixture (Singer 1981; Miyamoto *et al.* 1983; Cloutis *et al.* 1986; Cloutis and Gaffey 1991b) which limits the detailed quantitative mineralogical spectral analysis in this work. The only value from T-11 unit displays presence of orthopyroxene and olivine mixture that falls very near to olivine–pyroxene mixing line within OC region. Band parameter values in figure 5 show systematic gap in the data points that is marked with yellow and blue colour. This gap by the band parameter also signifies a systematic difference of the spatial mineralogical distribution within mare. Most of the yellow values present mafic mineralogy of the western deepest basin part of Mare Tranquillitatis (figure 6). Most of the blue coloured band parameter values cover eastern shield part of the mare and werstern most units of mare (T-1, T-16). Figure 6 locates this spatial distinction within mare. Trend line for the eastern mare band parameter indicates major variations in BAR values compared to variations in the Band I center. This trend marked by green trendline goes from calcic to high calcium pyroxene bearing region within the graph (figure 5). However, red trend line shows comparatively less variations in BAR ratio and more variation in band center values. Band parameter trend for the western part of the mare goes towards olivine bearing region in figure 5. This analysis indicates that basalts of eastern shield mare would have been comparatively more pyroxene bearing compared to the basalts from western deepest part, which would have been more olivine bearing compared to the eastern shield mare basalt.

5.3 *Composition of irregular mare patches*

Braden *et al.* (2014) mapped Irregular Mare Patches (IMPs) as evidence of recent volcanism within past 100 million year. From the total of IMPs, 51% (36 out of 70) IMPs were identified within the Mare Tranquillitatis. All these IMPs range in size from 100 to 5000 m. To study the composition of this IMPs, spectral reflectance profiles were collected very carefully from the M^3 100 and 200 km datasets. Figure 7 shows representative spectra of the 10 IMPs of Mare Tranquillitatis, which are collected from the locations marked in figure 8. In the spectra, Band I is less prominent and Band II is more prominent. Band I shows less strength and the center varies from 0.97 to 1.04 μm. Most of these centers also show clear two secondary side absorptions like olivine (figure 7, graph: c, d, e, f and spectra: 2c). However, B I center in figure 7, graph-a (except 2c), figure 7, graph-b, do not show this side wings. Band II displays very broad, prominent absorption with center range from 2.17 to 2.25 μm, which indicates presence of Chromite as per Cloutis *et al.* (2004). Spinel displays band II center up to 2.1 μm and longward shift of this feature (>2.1 μm) is ascribed to Chromite (Cloutis *et al.* 2004). Nature of the spectral reflectance profiles indicate that IMPs comprise olivine and chromite mixture bearing composition. Location, size and details of the IMPs are given in appendix III.

5.4 *Geomorphological investigation*

Eastern and western mare units show a significant spatial variation for the basaltic units, which may have raised due to the major topographic difference between eastern and western Mare Tranquillitatis. LROC LOLA topographic map is shown in figures 8 and 9. To study the spatial distribution of the spectral units, we overlaid the basaltic units on the topographic map presented in figure 8. Figure 9 presents major morphological and tectonic feature of mare, such as wrinkle ridges, sinus rille, domes, fault and collapsed pit. These features are digitized using LROC WAC data and overlaid on the topographic map. The study area presents two major topographic differences. Eastern topographic rise shows ∼2 km elevation difference compared to western deepest part. Spudis *et al.* (2011) had reported this eastern rise of Mare Tranquillitatis as the largest shield volcano on the Moon. Blue to green colour shows this Cauchy

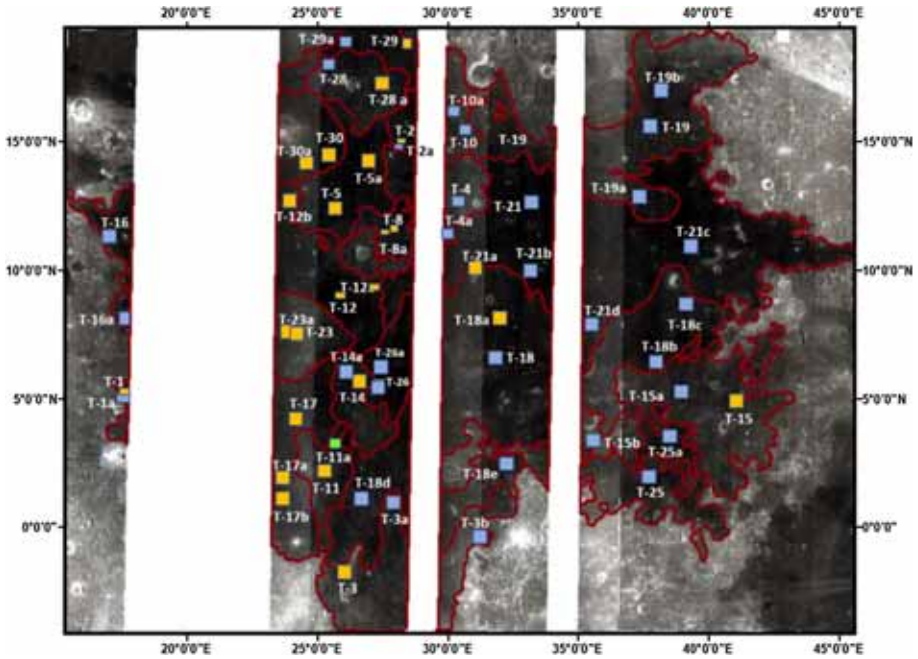

Figure 6. Location of all the spectral reflectance profiles of the basaltic units which are colour coded as per two different compositional trends observed in BAR *vs.* B I center plot in figure 5.

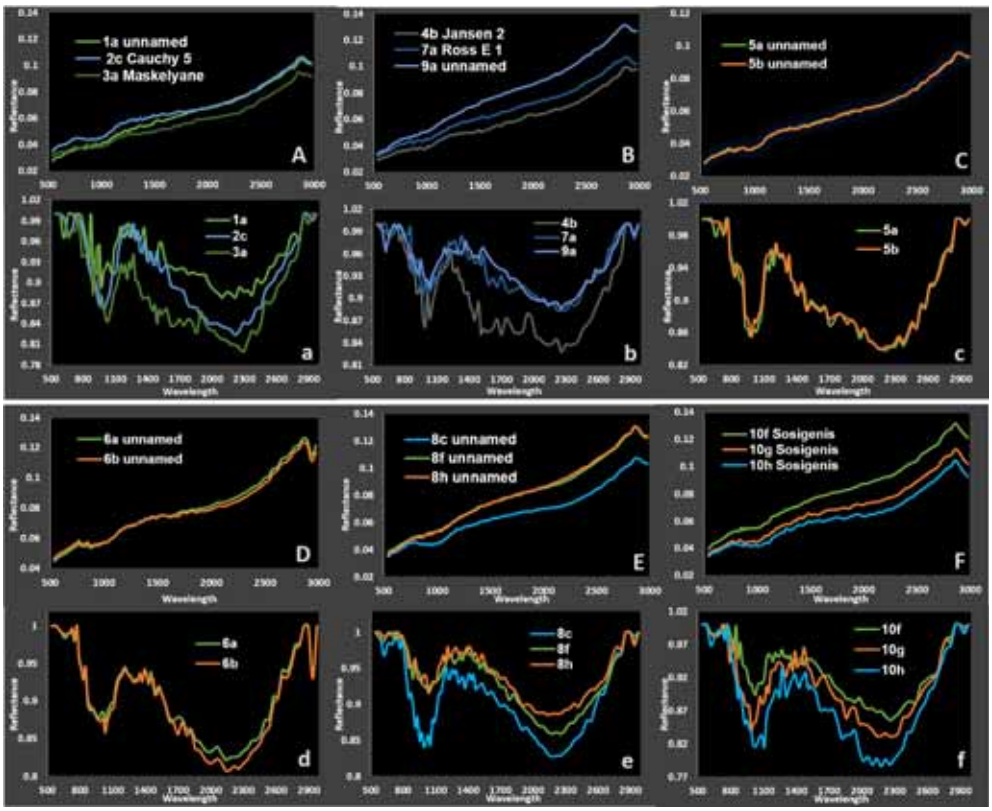

Figure 7. Normal (Graph: A, B, C, D, E, F) and Continuum removed (Graph: a, b, c, d, e, f) spectral reflectance profile of 10 representative Irregular Mare patches (IMPs) of Mare Tranquillitatis. Location map of these IMPs is given in the figure 8

shield plateau marked with maroon circle in figure 8. This shield presents two largest basaltic units T-21 and T-18 of this mare and some parts of T-15 and T-19 units. T-19, T-15, T-25, T-4, T-8, T-10 and T-18 shows ~ -2 to -3 km topographic relief. Units T-17 and T-23 show the deepest part

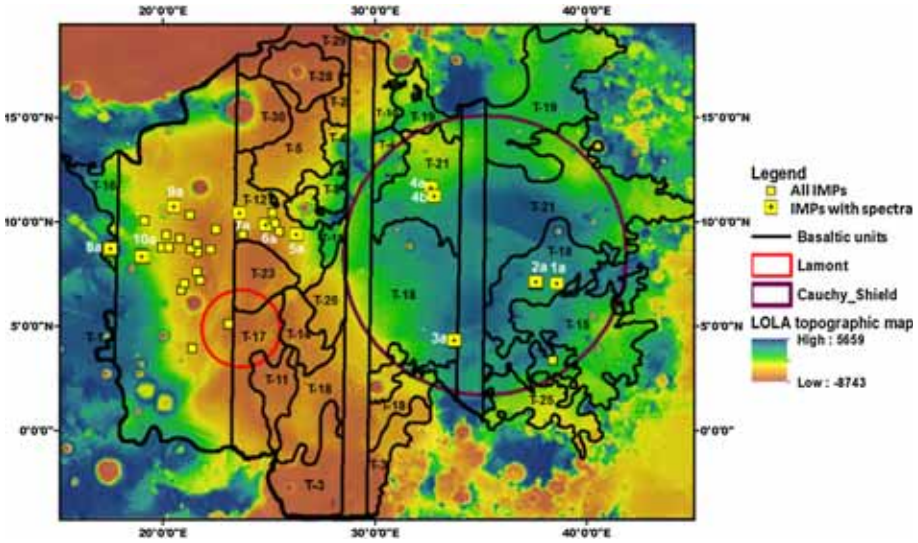

Figure 8. Topographic map of Mare Tranquillitatis generated using LRO LOLA DEM data of 29.61 m/pix resolution. Mare basaltic units have been overlaid on LOLA topographic map presented with black lines. Yellow square marks the location of the IMPs analysed in this work. Maroon circle in the eastern mare shows the boundary of Cauchy shield (from Spudis *et al.* 2013). Red circle is Lamont region.

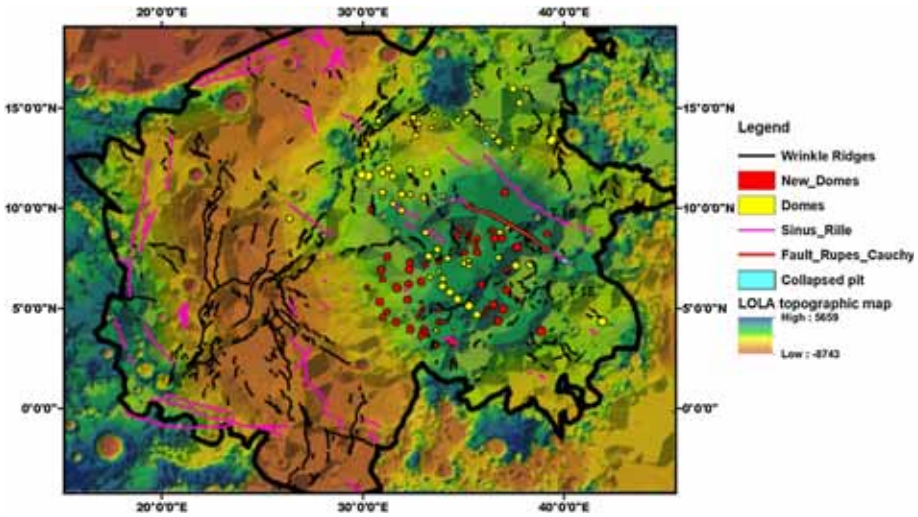

Figure 9. Topographic and morphological map of Mare Tranquillitatis generated using LRO LOLA DEM data of 29.61 m/pix resolution overlaid by major morphological and tectonic features.

of the area which is the Lamont region marked with a red circle (figure 8). This region shows topographic low near about −5 km. Lamont mascon region exhibits 72 km diameter ghost ring, lies along north–south trending linear anomaly associated with the Oceanus Procellarum region which is interpreted as a frozen remnant of the regional magmatic plumbing system (Neumann *et al.* 2015). Wrinkle ridges show circular concentric pattern in the Lamont region and large discontinuous circular pattern at the boundary of shield rise on the eastern part, which is presented in figure 9. The heights of wrinkle ridges in the radial group range from 60 to 490 m with an average height of 166.9 m and the average length is 23.04 km (Li *et al.* 2018). The ridge system in Tranquillitatis yields an average formation time of 2.4 Ga, which is 1.4 Ga after its oldest surface lavas, which spanned for significantly longer period than for any other basin (Li *et al.* 2018). Wilhelms *et al.* (1987) suggested that a pre-mare crater perched on this ring created the circular part of the ridge pattern, contains sufficient basalt to appear as a mascon, and remained elevated while subsidence crumpled the surrounding basalt flows into a radial ridge pattern at the Lamont region. Tye and Head (2013) have mapped 115 mare domes and showed that they are distributed highly inhomogeneously in the study

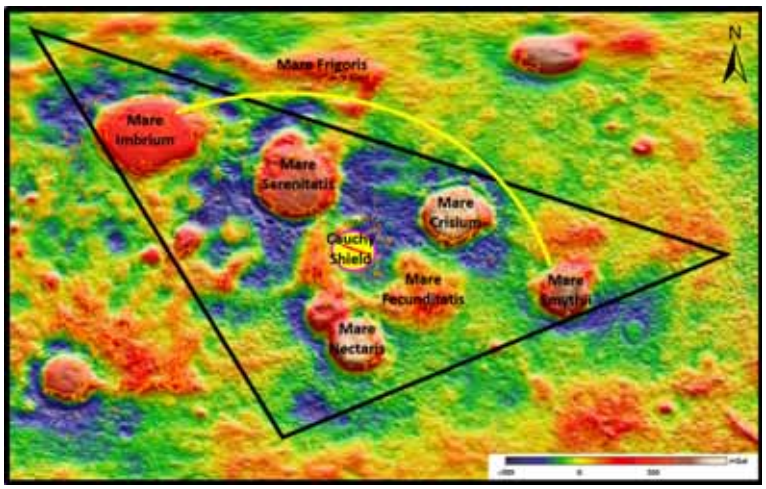

Figure 10. GRAIL Bouguer gravity anomaly map (https://quickmap.lroc.asu.edu), marked with triangular zone made by major eastern mascon basin centered by Cauchy shield (yellow circle) of Mare Tranquillitatis. Red line within the Cauchy shield marks major fault of the area, parallel to axis of the triangle.

area (Mare Tranquillitatis and parts of Serenitatis, Nectaris, Fecunditatis, and Crisium) and are associated with a large broad rise in the Maria, elevated up to 2.2 km above the surrounding mare regions. They investigated that 77 of the 115 domes (67%) reside within the eastern rise covering the area 1.5×10^5 km^2. This study investigated 61 new domes in the Cauchy shield region which is marked with red circles in figure 9. More number of domes indicate more intrusive activities in the region. Previously identified domes (Yellow) and new domes make linear pattern at north, and south part of the shield area, which runs parallel to the fault plain directed NW–SE. Most of the Sinus Rille run parallel to western most boundary of the mare and one longer rille runs parallel to Rupes Cauchy fault in the shield area figure 9.

5.5 *Possible formation and evolution of the basin*

Mare Tranquillitatis is positioned at unique location on the eastern near side. All the circular mascon basin, on the eastern near side, make unique triangular geometry which gives the exact or most acceptable reason for comprising the largest shield volcano on this one plate planetary body. GRAIL map of Bouguer gravity anomaly (https://quickmap.lroc.asu.edu) (figure 10) displays mascon basin surrounded by Mare Tranquillitatis. Recent GRAIL analysis suggests that western Lamont mascon is a frozen remnant of the regional magmatic plumbing system (Neumann *et al.* 2015) which starts from Oceanus procellarum to north at the Mare Frigoris and comes down to western part of Mare Tranquillitatis. This system has played major role in the formation of Lamont mascon region of western part of mare. Formation of the non-mascon Cauchy shield interpreted from the geometry marked in figure 10. The Cauchy shield of eastern part is the center-most location, where the stresses induced by the formation of surrounding impact basins (Imbrium, Serenitatis, Nectraris, Crisium, and Smythi) got centered and made a pressure relief zone at this location. This centroid location generated the magmatic cumulate zone of greater size beneath the surface, which erupted on the surface with time and formed the Cauchy shield. The results are in agreement with the previous works (Zuber *et al.* 2013; Tye and Head 2013), which suggest that mantle upliftment would not have played any role for the formation of the Cauchy shield. But, it is formed due to high pressure and stresses generated at the centroid by all the surrounded eastern mare basins, marked by triangle in the figure 10. The longest Rupes Cauchy faults (red line within Cauchy shield circle, figure 10), aligned domes (presented in figure 9), and longest Rima Cauchy rille (figure 9) in the Cauchy shield are parallel to the triangle edge which runs from the Mare Serenitatis to the Mare Smythi basin (figure 10). That signifies the stress zones within this area and its directions are aligned with the edge of this triangle.

6. Conclusions

This work has studied detailed compositional mapping of Mare Tranquillitatis basalt using hyperspectral M^3 data. Composition of Irregular

Mare Patches is also studied for the first time using M^3 data in this work. In the Cauchy shield area, 61 new domes have been identified over the previously identified number of domes. An attempt is made to understand possible origin and evolution of the Cauchy shield volcano.

Mare Tranquillitatis presents unique volcanic, tectonic and evolutionary history. This area marks more than 50% of the IMPs, which indicates that this older mare has remained volcanically more active for the longest geological period compared to all other mares of the Moon. Within the mare, western deepest part is older in formation which preserves all the larger craters of the area that belongs to pre-mare and post-mare formation. This western mare remained volcanically active for longest period as it comprises 28 IMPs in the T-12 unit, compared to eastern rise which is younger in age. All the other areas of this mare comprise only eight IMPs. Detailed spectral analysis of the Mare Tranquillitatis using IBD parameter technique delineates mare basalt units into 22 spectral segments. Spectral sampling from number of small fresh craters of each unit shows presence of olivine and sub-calcic pyroxene mixture bearing basaltic material. Eastern and western mare shows major topographic difference, spatial distribution difference of spectral units and also shows compositional difference trend in the BAR *vs.* B I center plot. Western mare shows more olivine bearing material in the olivine pyroxene mixture and the eastern mare displays more pyroxene bearing material in the olivine pyroxene mixture. Eastern mare shows more number of spectral units with smaller size compared to less numbered and larger units marked in the eastern mare. The Cauchy shield covers the largest spectral unit of the area (T-18 and T-21) which indicates the longest possible lava flow in the shield area. Western mare is older in age and the source region for the basalt of this area would have been deeper, compared to eastern mare shield that is comparatively younger. The youngest IMPs in the mare are composed of olivine and chromite bearing mineral mixtures, which significantly differs in composition from the underlying older mare basalt composition. The shield area marks number of domes, which are indicative of tectonic and intrusive volcanic activities in the period of post-mare formation. The largest shield volcano of the Moon-Cauchy shield covered by this mare lies on the unique location that makes centroid from all the eastern nearside mare basin of the Moon. The location of the Cauchy shield volcano signifies the most possible main cause for formation of the largest shield volcano, on this one plate planetary body – the Moon.

Acknowledgements

Authors are thankful to the Indian Space Research Organization (ISRO), India for financial support under the CH-1 AO Research project B.19013/39/2016-sec.2. The authors are also grateful to Satadru Bhattacharya and Mamta Chauhan for their valuable suggestions during the preparation of the manuscript and to the anonymous reviewers for their valuable suggestions, which greatly enhanced this manuscript.

References

Adams J B 1974 Visible and near-infrared diffuse reflectance spectra of pyroxenes as applied to remote sensing of solid objects in the Solar System; *J. Geophys. Res.* **79** 4829–4836.

Adams J B 1975 Interpretation of visible and near-infrared diffuse reflectance spectra of pyroxenes and other rock-forming minerals; In: *Infrared and Raman Spectroscopy of Lunar and Terrestrial Minerals* (ed.) Karr C III, Academic Press, New York, pp. 91–116.

Basaltic Volcanism Study Project (BVSP) 1981 *Basaltic volcanism on the terrestrial planets*; New York: Pergamon Press.

Beaty D W and Albee A L 1978 Comparative petrology and possible genetic relations among the Apollo 11 basalt; *Proc. Lunar Planet. Sci.* **9** 359–463.

Bell III J F and Hawke B R 1995 Compositional variability of the Serenitatis/Tranquillitatis region of the Moon from telescopic multispectral imaging and spectroscopy; *Icarus* **118(1)** 51–68.

Besse S, Sunshine J, Staid M, Boardman J, Pieters C, Guasqui P, Malaret E, McLaughlin A, Yokota Y and Li J Y 2013 A visible and near-infrared photometric correction for Moon Mineralogy Mapper (M^3); *Icarus* **222(1)** 229–242.

Bhatt H V, Solanki P M and Chauhan M 2018 Mineralogical and geomorphological mapping of western central part of Mare Tranquillitatis using hyperspectral imager onboard Chandrayaan-1; *IJRAT* **6** 1296–1301.

Bhatt H, Chauhan P, Bhattacharya S, Chauhan M and Solanki P 2019 Comparative spectral analysis approach: The study of Lunar Mineralogy using two hyperspectral data from Chandrayaan-1; *In: 50th Proc. Lunar Planet. Sci.* 2364.

Boardman J W, Pieters C M, Green R O, Lundeen S R, Varanasi P, Nettles J, Petro N, Isaccson P, Besse S and Taylor L A 2011 Measuring moonlight: An overview of the spatial properties, lunar coverage, selenolocation, and related Level 1B products of the Moon Mineralogy Mapper; *J. Geophys. Res.: Planet* **116(E6)**.

Braden S E, Stopar J D, Robinson M S, Lawrence S J, Van Der Bogert C H and Hiesinger H 2014 Evidence for basaltic

volcanism on the Moon within the past 100 million years; *Nat. Geosci.* **7(11)** 787.

Burns R G 1989 Spectral mineralogy of terrestrial planets: Scanning their surfaces remotely; *Mineral. Mag.* **53** 135–151.

Burns R G 1993 *Mineralogical applications of crystal field theory*; 2nd edn, Cambridge: Cambridge University Press, 523p.

Charette M P, McCord T B, Pieters C and Adams J B 1974 Application of remote spectral reflectance measurements to lunar geology classification and determination of titanium content of lunar soils; *J. Geophys. Res.* **79(11)** 1605–1613.

Chauhan P, Kaur P, Srivastava N, Bhattacharya S, Ajai, Kiran Kumar A S and Goswami J N 2012 Compositional and morphological analysis of high-resolution remote sensing data over central peak of Tycho crater on the Moon: Implications for understanding lunar Interior; *Curr. Sci.* **102(7)** 1041–1046.

Chauhan M, Bhattacharya S, Pathak S and Chauhan P 2018 Remote spectral–compositional analysis of basalt mineralogy at Hansteen-Billy, Moon; *Meteor. Planet. Sci.* **53(12)** 2583–2595.

Clark R N and Roush T L 1984 Reflectance spectroscopy: Quantitative analysis techniques for remote sensing applications; *J. Geophys. Res.: Solid Earth* **89(B7)** 6329–6340.

Clark R N, Pieters C M, Green R O, Boardman J W and Petro N E 2011 Thermal removal from near-infrared imaging spectroscopy data of the Moon; *J. Geophys. Res.: Planets* **116(E6)**.

Cloutis E A, Gaffey M J, Jackowski T L and Reed K L 1986 Calibrations of phase abundance, composition, and particle size distribution for olivine–orthopyroxene mixtures from reflectance spectra; *J. Geophys. Res.: Solid Earth* **91(B11)** 11,641–11,653.

Cloutis E A and Gaffey M J 1991a Pyroxene spectroscopy revisited – Spectral compositional correlations and relationship to geothermometry; *J. Geophys. Res.* **96** 22,809–22,826.

Cloutis E A and Gaffey M J 1991b Spectral-compositional variations in the constituent minerals of mafic and ultramafic assemblages and remote sensing implications; *Earth Moon Planets* **53(1)** 11–53.

Cloutis E A, Sunshine J M and Morris R V 2004 Spectral reflectance-compositional properties of spinels and chromites: Implications for planetary remote sensing and geothermometry; *Meteor. Planet. Sci.* **39(4)** 545–565.

Crown D A and Pieters C M 1987 Spectral properties of plagioclase and pyroxene mixtures and the interpretation of lunar soil spectra; *Icarus* **72** 492–506.

De Hon R A 2017 A two-basin model for Mare Tranquillitatis; *Proc. Lunar Planet. Sci.* **48**.

Dhingra D, Pieters C M, Isaacson P, Staid M, Mustard J, Klima R, Taylor L A, Kramer G, Nettles J and M^3 team 2010 Spectroscopic signature of the high titanium basalts at Mare Tranquillitatis from moon mineralogy mapper (M^3); *In: Proc. Lunar Planet. Sci.* XXXXI, Abstract 2494.

Elder C M, Hayne P O, Bandfield, J L, Ghent R R, Williams J P, Hanna K D and Paige D A 2017 Young lunar volcanic features: Thermophysical properties and formation; *Icarus* **290** 224–237.

Gaffey M J, Bell J F, Brown R H, Burbine T H, Piatek J L, Reed K L and Chaky D A 1993 Mineralogical variations within the S-type asteroid class; *Icarus* **106(2)** 573–602.

Gaffey M J, Cloutis E A, Kelley M S and Reed K L 2002 Mineralogy of asteroids; In: Asteroids III (eds) Bottke W F, Cellino A, Paolicchi P and Binzel R P, Tucson, Arizona: The University of Arizona Press, pp. 183–204.

Giguere T A, Taylor G J, Hawke B R and Lucey P G 2000 The titanium contents of lunar Mare basalts; *Meteor. Planet. Sci.* **35(1)** 193–200.

Gillis J J, Jolliff B L and Elphic R C 2003 A revised algorithm for calculating TiO_2 from Clementine UVVIS data: A synthesis of rock, soil, and remotely sensed TiO_2 concentrations; *J. Geophys. Res.: Planets* **108(E2)**.

Goswami J N and Annadurai M 2009 Chandrayaan-1: India's first planetary science mission to the Moon; *Curr. Sci.* **96** 486–491.

Head III J W 1976 Lunar volcanism in space and time; *Rev. Geophys.* **14(2)** 265–300.

Hiesinger H, Jaumann R, Neukum G and Head III J W 2000 Ages of Mare basalts on the lunar nearside; *J. Geophys. Res.: Planets* **105(E12)** 29,239–29,275.

Hollister L S and Hargraves R B 1970 Compositional zoning and its significance in pyroxenes from two coarse grained Apollo 11 samples; *Geochim. Cosmochim. Acta (Suppl.)* **1** 541.

Jerde E A, Snyder G A, Taylor L A, Yun-Gang L and Schmitt R A 1994 The origin and evolution of lunar high-Ti basalts: Periodic melting of a single source at Mare Tranquillitatis; *Geochim. Cosmochim. Acta* **58(1)** 515–527.

Johnson J R, Larson S M and Singer R B 1991 Remote sensing of potential lunar resources: 1. Near-side compositional properties; *J. Geophys. Res.: Planets* **96(E3)** 18,861–18,882.

Kaur P, Bhattacharya S, Chauhan P and Kumar A K 2013 Mineralogy of Mare Serenitatis on the near side of the Moon based on Chandrayaan-1 Moon Mineralogy Mapper (M^3) observations; *Icarus* **222(1)** 137–148.

King T V and Ridley W I 1987 Relation of the spectroscopic reflectance of olivine to mineral chemistry and some remote sensing implications; *J. Geophys. Res.* **92** 11,457–11,469.

Klima R L, Pieters C M and Dyar M D 2007 Spectroscopy of synthetic Mg–Fe pyroxenes I: Spin-allowed and spin-forbidden crystal field bands in the visible and near-infrared; *Meteor. Planet. Sci.* **42(2)** 235–253.

Klima R L, Dyar M D and Pieters C M 2011a Near-infrared spectra of clinopyroxenes: Effects of calcium content and crystal structure; *Meteor. Planet. Sci.* **46(3)** 379–395.

Klima R L, Pieters C M, Boardman J W, Green R O, Head J W, Isaacson P J, Mustard J F, Nettles J W, Petro N E, Staid M I, Sunshine J M, Taylor L A and Tompkins S 2011b New insights into lunar petrology: Distribution and composition of prominent low-Ca pyroxene exposures as observed by the Moon Mineralogy Mapper (M^3); *J. Geophys. Res.: Planets* **116(E6)**.

Kodama S and Yamaguchi Y 2003 Lunar Mare volcanism in the eastern nearside region derived from Clementine UV/VIS data; *Meteor. Planet. Sci.* **38(10)** 1461–1484.

Li B, Ling Z, Zhang J, Chen J, Ni Y and Liu C 2018 Displacement-length ratios and contractional strains of lunar wrinkle ridges in Mare Serenitatis and Mare Tranquillitatis; *J. Struct. Geol.* **109** 27–37.

Lucey P G, Taylor G J and Malaret E 1995 Abundance and distribution of iron on the Moon; *Science* **268(5214)** 1150–1153.

Melendrez D E, Johnson J R, Larson S M and Singer R B 1994 Remote sensing of potential lunar resources: 2. High spatial resolution mapping of spectral reflectance ratios and implications for nearside Mare TiO_2 content; *J. Geophys. Res.: Planets* **99(E3)** 5601–5619.

Miyamoto M, Kinoshita M and Takano Y 1983 Spectral reflectance (0.25–2.5 μm) of olivine and pyroxene from an ordinary chondrite; *Mem. Natl. Inst. Polar Res., Spec. Issue* **30** 367–377.

Muller P M and Sjogren W L 1968 Mascons: Lunar mass concentrations; *Science* **161(3842)** 680–684.

Mustard J F, Pieters C M, Issacson P J, Head J W, Besse S, Clark R N, Klima R L, Petro N E, Staid M I, Sunshine J M, Runyon C J and Tompkin S 2011 Compositional diversity and geologic insights of the Aristarchus crater from Moon Mineralogical Mapper data; *J. Geophys. Res.* **116** E00G12.

Nyquist L E and Shih C Y 1992 The isotopic record of lunar volcanism; *Geochim. Cosmochim. Acta* **56(6)** 2213–2234.

Neumann G A, Zuber M T, Wieczorek M A, Head J W, Baker D M, Solomon S C and Goossens S J 2015 Lunar impact basins revealed by gravity recovery and interior laboratory measurements; *Science Adv.* **1(9)** e1500852.

Papike J J, Hodges F N, Bence A E, Cameron M and Rhodes J M 1976 Mare basalts: Crystal chemistry, mineralogy, and petrology; *Rev. Geophys.* **14(4)** 475–540.

Pieters C M 1978 Mare basalt types on the front side of the moon – A summary of spectral reflectance data; *Proc. Lunar Planet. Sci.* **9** 2825–2849.

Pieters C M 1993 Compositional diversity and stratigraphy of the lunar crust derived from reflectance spectroscopy; *Remote Geochemical Analysis Elemental and Mineralogical Composition*, pp. 309–339.

Pieters C M and Englert P A (eds) 1997 *Elemental and Mineralogical Composition*; Cambridge University Press, New York.

Pieters C M, Boardman J, Buratti B, Chatterjee A, Clark R, Glavich T, Green R, Head J III, Isaacson P, Malaret E, McCord T, Mustard J, Petro N, Runyon C, Staid M, Sunshine J, Taylor L, Tompkins S, Varanasi P and White M 2009 The Moon Mineralogical Mapper (M3) on Chandrayaan-1; *Curr. Sci.* **96** 500–505.

Sato H, Robinson M S, Lawrence S J, Denevi B W, Hapke B, Jolliff B L and Hiesinger H 2017 Lunar Mare TiO_2 abundances estimated from UV/Vis reflectance; *Icarus* **296** 216–238.

Singer R B 1981 Near-infrared spectral reflectance of mineral mixtures: Systematic combinations of pyroxenes, olivine, and iron oxides; *J. Geophys. Res.* **86** S7967–S7982.

Snyder G A, Lee D C, Taylor L A, Jerde E A and Halliday A N 1992 March Nd and SR Isotopic constraints on high-Ti basalt volcaniosm at Mare Tranquillitatis; *Proc. Lunar Planet. Sci.* **23**.

Spudis P D 2005 *The geology of multi-ring impact basins: The Moon and other planets*; Cambridge University Press.

Spudis P D, McGovern P J and Kiefer W S 2011 Large shield volcanoes on the Moon; *LPSC* **42** Abstract 1367.

Spudis P D, McGovern P J and Kiefer W S 2013 Large shield volcanoes on the Moon; *J. Geophys. Res.: Planets* **118(5)** 1063–1081.

Staid M I, Pieters C M and Head III J W 1996 Mare Tranquillitatis: Basalt emplacement history and relation to lunar samples; *J. Geophys. Res.: Planets* **101(E10)** 23,213–23,228.

Tye A and Head III J W 2013 March Mare Tranquillitatis: Distribution of Mare domes, relation to broad Mare rise, and evidence of a previously unrecognized basin from LOLA altimetric data; *In: Proc. Lunar Planet. Sci.* XLIV, abstract (Vol. 1319).

Wilhelms D E, John F and Trask N J 1987 The geologic history of the Moon; U.S. Geological survey professional paper (No. 1348).

Wilcox B B, Lucey P G and Gillis J J 2005 Mapping iron in the lunar Mare: An improved approach; *J. Geophys. Res.: Planets* **110(E11)**.

Wood C A 2003 *The modern Moon: A personal view*; Cambridge, MA: Sky Publishing Corporation, pp. 144–151.

Zuber M T, Smith D E, Watkins M M, Asmar S W, Konopliv A S, Lemoine F G, Jay Melosh H, Neumann G A, Phillips R J, Solomon S C, Wieczorek M A, Williams J G, Goosens S J, Kruizinga G, Mazarico E, Park R S and Yuan D N 2013 Gravity field of the Moon from the Gravity Recovery and Interior Laboratory (GRAIL) mission; *Science* **339(6120)** 668–671.

Corresponding editor: N V Chalapathi Rao